Inorganica Chimica Acta 391 (2012) 28–35

Contents lists available at SciVerse ScienceDirect

Inorganica Chimica Acta

journal homepage: www.elsevier.com/locate/ica

Synthesis, spectroscopic, magnetic and thermal properties of copper(II), nickel(II) and iron(II) complexes with some tetradentate ligands: Solvatochromism of iron(II)–L^2

Alper Onder [a], Murat Turkyilmaz [b], Yakup Baran [a,*]

[a] Onsekiz Mart University, Art and Science Faculty, Department of Chemistry, Canakkale 17100, Turkey
[b] Trakya University, Science Faculty, Department of Chemistry, Edirne, Turkey

ARTICLE INFO

Article history:
Received 10 February 2012
Received in revised form 27 April 2012
Accepted 10 May 2012
Available online 19 May 2012

Keywords:
Azomethines
Thermal stability
Spectroscopic
Solvatochromism
Complexes

ABSTRACT

The tetradentate azomethines were prepared by condensation of 2-piperazin-1-ylethanamine, (3-morpholin-4-ylpropyl)amine with 3-methylthophene-2-carbaldehyde, salicylaldehyde and 1*H*-imidazole-5-carbaldehyde. The ligands were characterized based on mass, ^{1}H and ^{13}C NMR, FTIR, and elemental analyses. New complexes of ligands with copper(II), iron(II) and nickel(II) were synthesized. Metal complexes are reported and characterized by magnetic, conductivity measurements, FTIR, elemental and thermal analyses (TG–DTA). Spectral analyses show that all the ligands behave as neutral tetradentate ligands and bind to the metal via azomethine N, piperazine N, salicylaldehyde O, morpholine O, imidazole N and thiophene S. Results of magnetic measurements and thermal studies show that the geometrical structures of the nickel(II) complexes are square planar while copper(II) and iron(II) are octahedral. The thermal behaviors of these complexes show that the hydrated complexes lose the hydration water molecule in the first step, followed immediately by decomposition of the anion and ligand molecules in subsequent steps. The solvatochromic behavior of the iron(II)–L^2 complex was investigated using the electronic spectra of 1×10^{-3} M in four different solvents. The solvatochromism was explained in terms of MLCT transition and solvent characteristics such as polarity, nature and acceptor–donor properties.

1. Introduction

The synthesis of a new ligand is the most important step in the development of metal complexes with unique properties and novel reactivity. Four tetradentate azomethines were prepared. L^3 and L^4 are new and L^2 is patented [1]. L^1 was prepared and its cadmium(II) and nickel(II) complexes were reported. These are X-ray structure reports and solution equilibrium respectively. Azomethines can be considered an important class of organic compounds which are good chelating agents because of the presence of both hard nitrogen and oxygen, and soft sulfur donor atoms in the backbones of these ligands [2]. Tetradentate azomethines, with N_2O_2 donor sets resulting from the condensation of aliphatic diamines, have been extensively studied [3–6]. Azomethine complexes are studied for their antitumor, antimicrobial, antiviral, catalytic, enzymatic and mesogenic characteristics [7–13]. Nickel–L^1 complex has been studied for planar-octahedral equilibrium in solution [14]. Synthesis, crystal structure, and magnetic properties of copper–L^2 were studied. The inhibitory bioactivities of nickel–L^2 against urease and xanthine have been studied [15,16]. Azomethine metal complexes are also a focus for scientific interest, due to their important role in biological systems, and represent an interesting model for metalloenzymes which efficiently catalyze the reduction of oxygen. Thermal decomposition of the metal complexes is used to infer the structures of the metal complexes together with the other spectroscopic and elemental analysis data [17–19]. Salicylaldehyde derivatives of azomethine compounds show a variety of biological activities, such as antibacterial activity [20]. The electronic spectra of the inorganic compounds can be affected by solvents. These complexes are usually referred to as solvatochromic substances and recent papers indicate continuing interest in this field [21–25]. The solutions of $[FeL^2Cl_2]$ range in color from yellow to purple in solvents. These colors are due to intense charge transfer bands involving electron transfer from the metal t_{2g} orbital in low spin d^6 to low lying π^* orbital in the azomethine. This color change occurs without any structural change in the chromophor. This is where the MLCT transition between iron(II) and azomethine takes place. Stronger acceptor properties of the solvent leads to a greater MLCT blue shift observed.

This work deals with the synthesis, characterization and thermal behavior of new tetradentate azomethine complexes of

---

* Corresponding author. Tel.: +90 286 2180018; fax: +90 286 2180533.
E-mail address: yakupbaran@yahoo.com (Y. Baran).

0020-1693/$ - see front matter © 2012 Elsevier B.V. All rights reserved.
http://dx.doi.org/10.1016/j.ica.2012.05.006

copper(II), nickel(II) and iron(II). Iron(II)–L^2 exhibits significant solvatochromic band shifts in certain solutions. In this paper we report the coordination behavior of azomethines toward these metal ions, thermal properties, spectroscopic properties of ligand and complexes, conductivity and solvatochromism of iron(II)–L^2.

2. Experimental

2.1. Materials

All chemicals used in this study were chemically pure (Aldrich). They were used without further purification. The organic solvent (methanol) was spectroscopic grade and all reactions were performed under argon atmosphere.

2.2. Physical measurements

The FTIR spectra of all ligands, which were obtained as oils, were recorded between KBr disks with a Perkin Elmer BXII FTIR spectrophotometer in wavenumbers of 4000–400 cm^{-1}. A small drop of the compound was placed on one of the potassium bromide plates and the second plate was placed on top and a quarter turn made to obtain a nice even film. The complexes were recorded by applying the KBr disc technique. ^1H and ^{13}C NMR spectra of the ligands were measured with a Varian 300 MHz spectrometer in $CDCl_3$ and CD_3OH, and chemical shifts are indicated in ppm relative to the solvent peak. The elemental analyses for the compounds were carried out using a Perkin Elmer PE 2400 C H N elemental analyzer. The mass spectra of the azomethines were measured by the EI technique on a Thermo Finnigan Trace DSQ spectrometer. Thermal stabilities of the complexes were examined using a Seiko SII TG–DTA 6300 thermal analyzer. The mass loss was measured from 25 up to 1200 °C at a heating rate of 15 °C min^{-1} in dynamic nitrogen atmosphere. The molar magnetic susceptibilities of the complexes were measured from a powdered sample at room temperature using a Sherwood Scientific Magnetic Susceptibility Balance. Metal analysis was carried out on a Perkin-Elmer 238 AAS. The effective magnetic moments were calculated as BM. The electronic spectra of the ligands and complexes were measured by an Agilent HP 8453 Diode Array UV–Vis spectrophotometer. The conductivity measurement was performed by a WTW inolab 720 conductometer. The residues of the TG–DTA study were analyzed by a Bruker D2 Phaser XRD.

2.3. Synthesis of the azomethines

All the tetradentate unsymmetrical azomethines were prepared by a similar method.

A solution of 15 mmol amine was dissolved in 50 mL methanol and 15 mmol aldehyde, dissolved in 40 mL methanol, was added to the amine solution on a magnetic stirrer at room temperature for 10 min then stirred for 4 h at 50 °C. The colored solution was concentrated in a rotary evaporator which produced a viscous oil. All the substances were checked for purity by thin layer chromatography and then loaded into a silica column for purification.

2.3.1. ***L***^{1}, *2-{(E)-[(2-piperazin-1-ylethyl) imino] methyl}phenol*

Anal. Calc. for $C_{13}H_{19}N_3O$ (233.31): C, 66.71; H, 8.29; N, 18.09. Found: C, 66.54; H, 8.33; N, 18.13%. ^1H NMR (300 MHz, $CDCl_3$) δ ppm: 8.30 (s, H, imine); 7.25 (d, H, J = 3 Hz); 7.21 (d, H, J = 3 Hz); 6.86 (double t, H, J = 6 Hz); 3.67 (t, 6H, J = 9 Hz); 2.39 (t, 6H, J = 6 Hz). ^{13}C ($CDCl_3$) δ ppm: 180.49 (C=N); 166.02 (C–OH); 161.37, 132.60; 131.52; 118.84; 117.26 (all aromatics), 58.67 (N–CH_2, 2C piperazin); 56.94(CH_2 aliphatic); 53.61 (HN–CH_2, 2C, piperazin); 51.61(CH_2 aliphatic). GS–MS (m/z): 234.05 $[M+H]^+$ calculated 233.31. FTIR (KBr, cm^{-1}): 3356 (OH), 1632 (C=N).

2.3.2. ***L***^{2}, *2-{(E)-[(3-morpholin-4-ylpropyl) imino]methyl}phenol*

Anal. Calc. for $C_{14}H_{20}N_2O_2$ (248.32): C, 67.72; H, 8.21; N, 11.33. Found: C, 67.77; H, 8.33; N, 11.40%. ^1H NMR (300 MHz, $CDCl_3$) δ ppm: 8.34 (s, imine); 7.29 (d, H, J = 3 Hz); 7.19 (d, H, J = 3 Hz); 6.83 (double t, 2H, J = 6 Hz); 3.73 (t, 4H, (morpholine, OCH_2) J = 9 Hz); 2.88 (t, 4H, J = 6 Hz); 2.67 (t, 2H, J = 6 Hz); 2.49 (t, 2H, J = 6 Hz) 13C ($CDCl_3$) δ ppm: 178.79 (C=N); 165.25 (C–OH); 161.46; 132.37; 131.36; 118.71; 117.21 (all aromatics), 67.18 (O–CH_2, 2C, morpholine); 57.57 (C, aliphatic); 56.52(N–CH_2, 2C, morpholine); 53.90 (CH_2, aliphatic); 27.80 (*CH_2*–CH_2–CH_2–). GS–MS (m/z): 249.00 $[M+H]^+$ calculated 248.32. FTIR (KBr, cm^{-1}): 3343 (OH), 1633 (C=N).

2.3.3. ***L***^{3}, *[(1E)-(3-methyl-2-thienyl)methylene](2-piperazin-1-ylethyl) amine*

Anal. Calc. for $C_{12}H_{19}N_3S$ (237.37): C, 60.71; H, 8.01; N, 17.74. Found: C, 60.55; H, 8.14; N, 17.71. ^1H NMR (300 MHz, $CDCl_3$) δ ppm: 8.41 (s, H, imine); 7.25 (d, H, aromatic, J = 3 Hz); 6.81 (d, H, aromatic, J = 6 Hz); 3.69 (t, 2H piperazine, J = 9 Hz); 2.85 (t, 4H aliphatic + piperazine, J = 6 Hz); 2.63 (t, 2H, aliphatic, J = 9 Hz); 2.48(s, 3H, CH_3); 2.33(t, 4H piperazine), J = 6 Hz). ^{13}C ($CDCl_3$) δ ppm: 178.67 (C=N); 154.30; 140.29; 130.88; 128.14 (aromatics); 59.77; 58.63 (N–CH_2, 2C, piperazine); 55.04; 46.27 (NH–CH_2, 2C, piperazine); 14.04 (CH_3). GS–MS (m/z): 237.99 $[M+H]^+$ calculated 237.37. FTIR (KBr, cm^{-1}): 1627 (C=N).

2.3.4. ***L***^{4}, *[(1E)-1H-imidazol-5-ylmethylene](2-piperazin-1-ylethyl) amine*

Anal. Calc. for $C_{10}H_{17}N_5$ (207.28): C, 58.03; H, 8.22; N, 33.82. Found: C, 57.91; H, 8.13; N, 33.77%. ^1H NMR (300 MHz, $CDCl_3$) δ ppm: 8.17 (s, H imine); 7.65 (s, H aromatic) 7.34 (s, H aromatic); 3.70 (double t, 4H aliphatic + piperazine, J = 9 Hz); 2.88 (quartet, t, 8H aliphatic + piperazine J = 6 Hz). ^{13}C ($CDCl_3$) δ ppm: 178.79 (C=N); 152.90; 114.89; 109.81 (aromatics); 60.07; 57.91 (N–CH_2, 2C); 54.96; 46.16 (NH–CH_2, 2C). GS–MS (m/z): 208.05 $[M+H]^+$ calculated 207.28. FTIR (KBr, cm^{-1}): 1632 (C=N).

2.4. Synthesis of the complexes

All the complexes were prepared by the same procedure as follows: 8 mmol metal chloride was dissolved in 50 mL argon saturated hot water–methanol mixture and the solution of azomethine 8 mmol in hot methanol was added slowly and stirred at 50 °C for 5 h to yield the azomethine metal complex, ML, as a precipitate. The precipitate was filtered and washed with cold ethanol several times. The solid was dried in vacuum desiccators and subjected to FTIR, UV–Vis and elemental analysis.

2.4.1. *Nickel–L^1 chloride tetrahydrate*

Yield: 67%. FTIR (KBr, cm^{-1}): 3367, 3033, 1627, 561 (M–N), 572 (M–O). UV–Vis (H_2O, nm; (ε, M^{-1} cm^{-1})): 352(1466), 481(566). *Anal.* Calc. for $C_{13}H_{27}N_3O_4Cl_2Ni$: C, 35.92; H, 6.12; N, 9.73. Found: C, 35.78; H, 5.83, N, 9.68%.

2.4.2. *Iron–L^1 chloride monohydrate*

Yield: 66%. FTIR (KBr, cm^{-1}): 3399, 3049, 1611, 542 (M–N), 566 (M–O). UV–Vis (H_2O, nm; (ε, M^{-1} cm^{-1})): 316(1334), 438(388). *Anal.* Calc. for $C_{13}H_{21}N_3O_2Cl_2Fe$: C, 41.42; H, 5.42; N, 11.14. Found: C, 41.34; H, 5.33; N, 11.20%.

2.4.3. *Copper–L^1 chloride monohydrate*

Yield: 81%. FTIR (KBr, cm^{-1}): 3435, 3022, 1635, 509 (M–N), 521 (M–O). UV–Vis (H_2O, nm; (ε, $M^{-1}cm^{-1}$)): 357(1240), 641(520).

Anal. Calc. for $C_{13}H_{21}N_3O_2Cl_2Cu$: C, 40.52; H, 5.21; N, 10.94. Found: C, 40.45; H, 5.27; N, 11.11%. Paramagnetic with 1.81 BM.

2.4.4. Nickel–L^2 chloride dihydrate

Yield: 47%. FTIR (KBr, cm^{-1}): 3367, 3010, 1628, 537 (M–N), 544 (M–O). UV–Vis (H_2O, nm; (ε, $M^{-1}\,cm^{-1}$)): 385(1355), 476(488). *Anal.* Calc. for $C_{14}H_{24}N_2O_4Cl_2Ni$: C, 38.83; H, 5.38; N, 7.04. Found: C, 38.74; H, 5.44; N, 6.94%.

2.4.5. Iron–L^2 chloride dihydrate

Yield: 61%. FTIR (KBr, cm^{-1}): 3399, 3025, 1613, 543 (M–N), 557 (M–O). UV–Vis (H_2O, nm; (ε, $M^{-1}\,cm^{-1}$)): 315(1223), 391(401). *Anal.* Calc. for $C_{14}H_{24}N_2O_4Cl_2Fe$: C, 39.32; H, 5.61; N, 7.02. Found: C, 39.17; H, 5.52; N, 7.10%.

2.4.6. Copper–L^2 chloride monohydrate

Yield: 68%. FTIR (KBr, cm^{-1}): 3354, 3019, 1640, 556 (M–N), 568(M–O). UV–Vis (H_2O, nm; (ε, $M^{-1}\,cm^{-1}$)): 355(1113), 556(396). *Anal.* Calc. for $C_{14}H_{22}N_2O_3Cl_2Cu$: C, 38.42; H, 5.29; N, 6.93. Found: C, 38.35; H, 5.37; N, 6.96%. Paramagnetic with 1.62 BM.

2.4.7. Iron–L^3 chloride monohydrate

Yield: 53%. FTIR (KBr, cm^{-1}): 3019, 1629, 507 (M–N). UV–Vis (H_2O, nm; (ε, $M^{-1}\,cm^{-1}$)): 366(1277), 482(388). *Anal.* Calc. for $C_{12}H_{21}N_3OSCl_2Fe$: C, 37.82; H, 5.33; N, 11.04. Found: C, 37.73; H, 5.23; N 11.20%.

2.4.8. Copper–L^3 chloride dihydrate

Yield: 67%. FTIR (KBr, cm^{-1}): 3021, 1652, 510 (M–N). UV–Vis (H_2O, nm; (ε, $M^{-1}\,cm^{-1}$)): 281(1322), 510(411). *Anal.* Calc. for $C_{12}H_{23}N_3O_2SCl_2Cu$: C, 35.42; H, 5.40; N, 10.33. Found: C, 35.29; H, 5.34; N, 10.40%. Paramagnetic with 1.96 BM.

2.4.9. Nickel–L^4 chloride pentahydrate

Yield: 67%. FTIR (KBr, cm^{-1}): 3035, 1627, 524 (M–N). UV–Vis (H_2O, nm; (ε, $M^{-1}\,cm^{-1}$)): 260(1221), 484(377). *Anal.* Calc. for $C_{10}H_{27}N_5O_5Cl_2Ni$: C, 28.13; H, 5.90; N, 16.53. Found: C, 28.06; H, 5.82; N, 16.50%.

2.4.10. Iron–L^4 chloride monohydrate

Yield: 67%. FTIR (KBr, cm^{-1}): 3031, 1629, 535 (M–N). UV–Vis (H_2O, nm; (ε, $M^{-1}\,cm^{-1}$)): 345(1123), 485(298). *Anal.* Calc. for

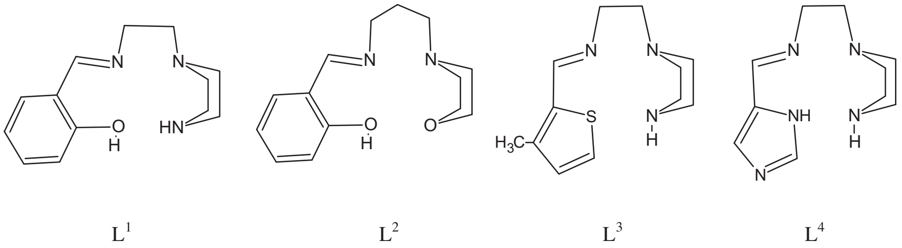

Scheme 1. Structures of the ligands.

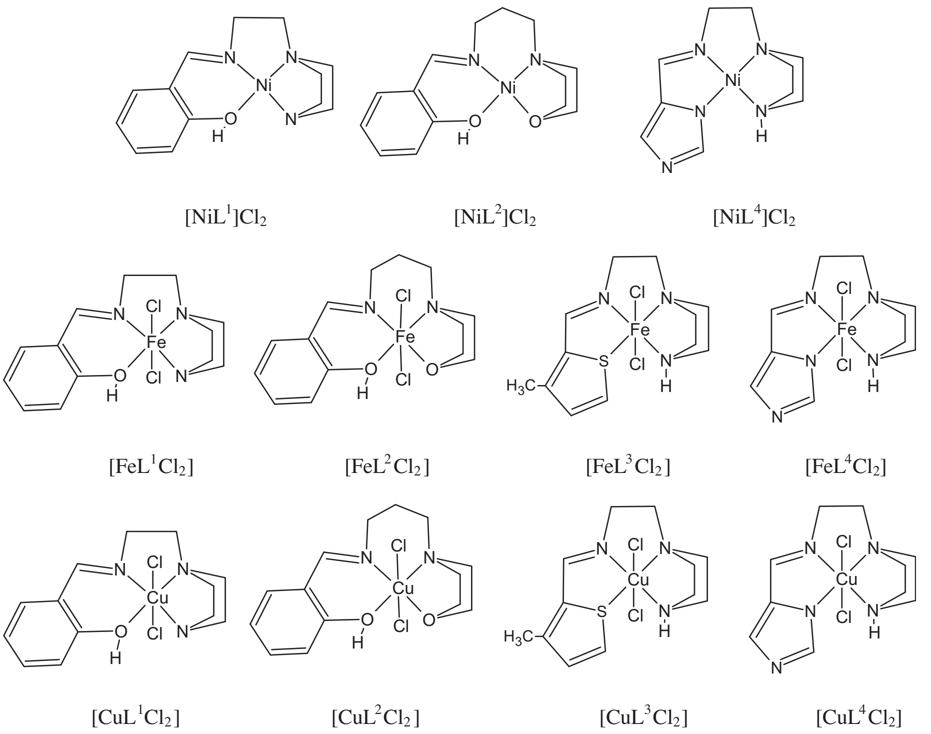

Scheme 2. Proposed structures of the complexes.

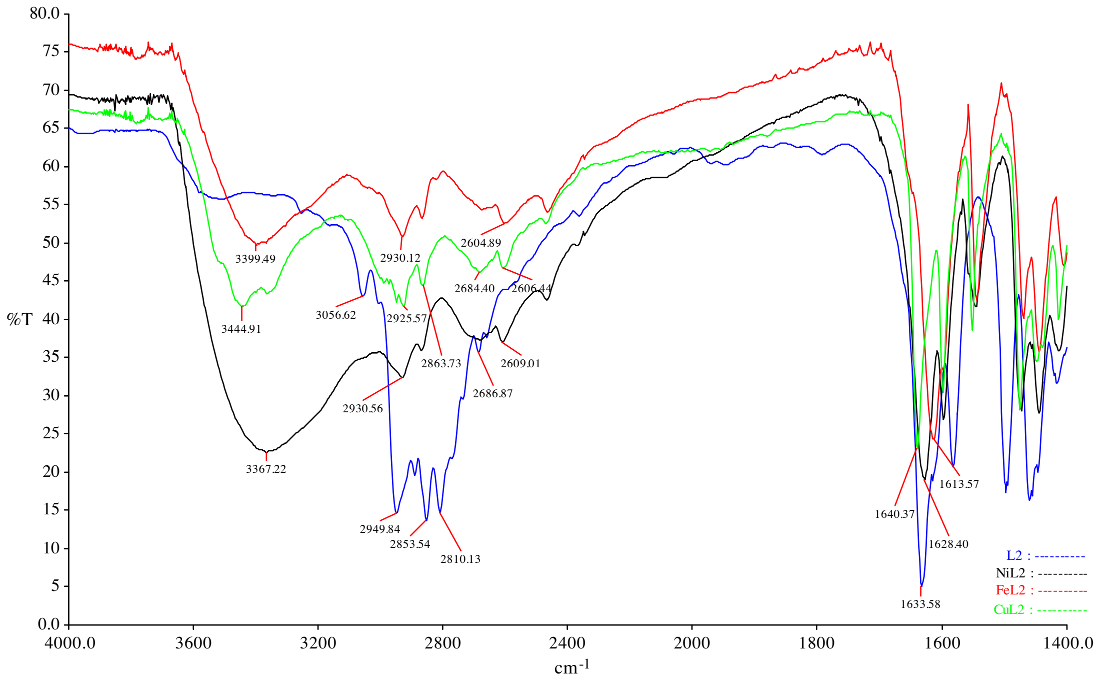

Fig. 1. FTIR spectra of the Ni(II), Fe(II) and Cu(II) complexes of L^2.

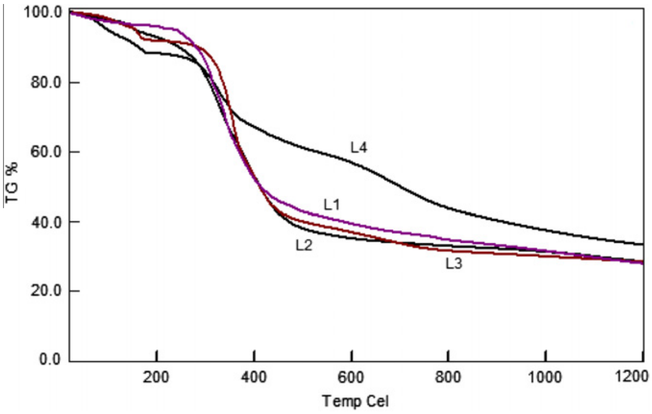

Fig. 2. TG curves of the Cu(II) complexes of L^1, L^2, L^3 and L^4.

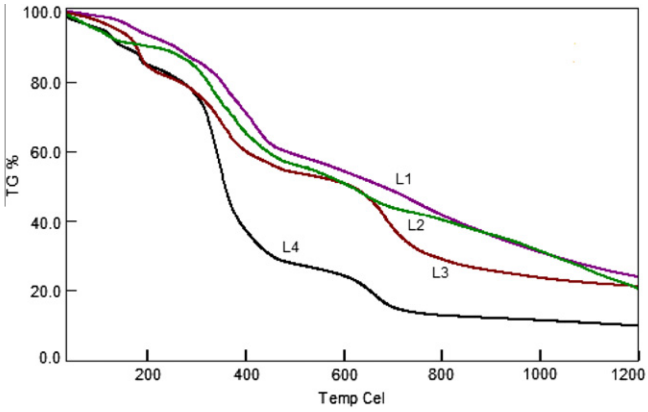

Fig. 3. TG curves of the Fe(II) complexes of L^1, L^2, L^3 and L^4.

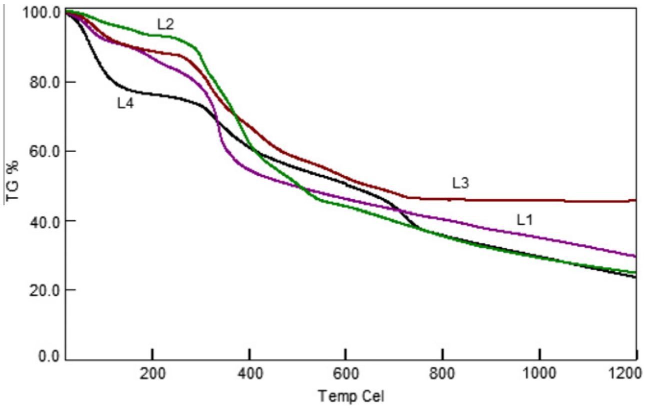

Fig. 4. TG curves of the Ni(II) complexes of L^1, L^2, L^3 and L^4.

$C_{10}H_{19}N_5OCl_2Fe$: C, 34.33; H, 4.93; N, 20.04. Found: C, 34.21; H, 4.93; N, 20.13%.

2.4.11. Copper–L^4 chloride trihydrate

Yield: 67%. FTIR (KBr, cm^{-1}): 3024, 1623, 518 (M–N). *Anal.* Calc. for $C_{10}H_{23}N_5O_3Cl_2Cu$: C, 30.34; H, 5.92; N, 17.73. Found: C, 30.37; H, 5.86; N, 17.75%. Paramagnetic with 1.55 BM.

3. Result and discussion

3.1. Elemental analysis of the complexes

The results of the elemental analyses are consistent with the results calculated from the empirical formulae of each compound. The structures of the ligands and their complexes are given in Schemes 1 and 2. The chloride salts of the metal were used in complex preparation. The complexes are stable, non-hygroscopic and soluble in water.

3.1.1. ^{1}H and ^{13}C NMR spectra

Azomethine protons have singlets at 8.34, 8.30, 8.41 and 8.17 ppm for L^1, L^2, L^3 and L^4, respectively. In the region 7.65–6.68 ppm chemical shifts were assigned to aromatic hydrogens. There were chemical shifts of aliphatic hydrogen in the region 3.73–1.84 ppm. L^1 has seven different carbons in the aromatic region and four peaks for aliphatic carbons. ^{13}C NMR of this ligand has seven peaks in between 180.49 and 117.26 and four peaks in between 58.67 and 51.61 ppm. The other ligands have the same trends for proton and ^{13}C NMR spectra.

3.2. Mass spectra of the azomethines

The electron impact mass spectra of the azomethines were recorded and investigated at 50 eV of electron energy. The important mass fragmentations and molecular ion peaks for the azomethines

Table 1
Thermal analysis data of the complexes.

Complexes	Step	Onset (°C)	DTG maximum (°C)	Endset (°C)	Leaving group	Mass loss (%)		Residue expt. (Calc.)
						Exp	Calc.	
$[CuL^1Cl_2]\cdot H_2O$	1	25		197	H_2O	4.00	4.48	CuO 28.20 (19.78)
	2	279	344	415	$L_1 + Cl_2$	67.40	75.73	
$[CuL^2Cl_2]\cdot H_2O$	1	25		132	H_2O	6.80	8.20	CuO 28.60 (18.66)
	2	132	146	162				
	3	280	327	456	$L_2 + Cl_2$	64.40	75.00	
$[CuL^3Cl_2]\cdot 2H_2O$	1	25		136	H_2O	8.20	8.48	CuO 28.70 (18.65)
	2	156	162	170				
	3	302	362	445	$L_3 + Cl_2$	62.80	72.77	
	4	587	693	755				
$[CuL^4Cl_2]\cdot 3H_2O$	1	25		177	H_2O	12.00	13.11	CuO 23.50 (19.30)
	2	282	329	362	$L_4 + Cl_2$	54.50	67.57	
	3	607	704	776				
$[FeL^1Cl_2]\cdot H_2O$	1	25		145	H_2O	6.00	4.56	FeO 24.30 (18.22)
	2	145	173	191				
	3	243	276	292	$L_1 + Cl_2$	68.40	77.20	
	4	340	366	455				
	5	653	807	931				
$[FeL^2Cl_2]\cdot 2H_2O$	1	25		116	H_2O	8.30	8.42	FeO 17.40 (16.82)
	2	116	126	142				
	3	275	364	430	$L_2 + Cl_2$	73.50	74.75	
	4	600	656	696				
$[FeL^3Cl_2]\cdot H_2O$	1	25		171	H_2O	4.00	4.52	FeO 21.60 (18.04)
	2	171	186	202	$L_3 + Cl_2$	74.40	77.47	
	3	284	352	478				
	4	636	683	729				
$[FeL^4Cl_2]\cdot H_2O$	1	25		118	H_2O	15.30	15.24	FeO 18.40 (17.38)
	2	118	127	138				
	3	179	187	191				
	4	298	344	448	$L_4 + Cl_2$	71.00	67.36	
	5	610	667	706				
$[NiL^1]Cl_2\cdot 4H_2O$	1	25		166	H_2O	14.40	14.75	NiO 27.00 (16.89)
	2	166	197	222				
	3	320	338	354	$L_1 + Cl_2$	58.2	68.84	
$[NiL^2]Cl_2\cdot 2H_2O$	1	25		157	H_2O	7.00	7.16	NiO 25.20 (17.74)
	2	157	170	187				
	3	272	381	409	$L_2 + Cl_2$	67.80	75.77	
	4	489	510	542				
$[NiL^4]Cl_2\cdot 5H_2O$	1	25		196	H_2O	21.20	20.36	NiO 18.80 (17.49)
	2	196	392	392	$L_4 + Cl_2$	59.10	62.95	
	3	392	725	756				

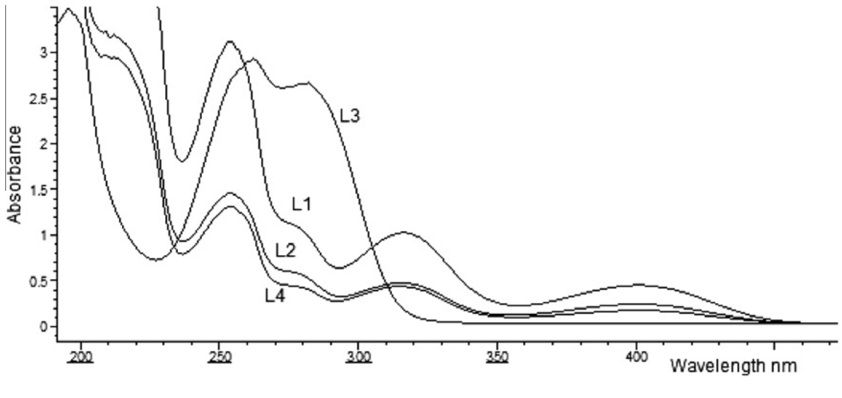

Fig. 5. Electronic spectra of the ligands.

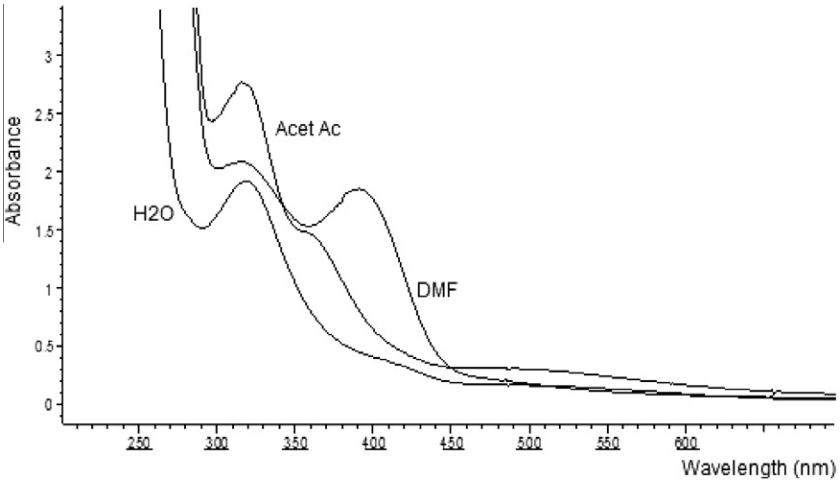

Fig. 6. Electronic spectra of the Fe–L^2 complex in H_2O, acetyl acetone and DMF.

are shown in the spectra. The mass spectra of these ligands are given as Supplementary information.

L^1: $m/z = 134$ peak was observed for the C_8H_8NO, OH-C_6H_4–CH═N–CH_2^+. The base peak is observed at $m/z = 99$ for the $C_5H_{11}N_2$, CH_3 attached to piperazine ring. The $m/z = 84$ for the $C_4H_8N_2$ for the piperazine ring. The $m/z = 70$ for the $C_3H_6N_2$ for the piperazine ring fragmentation.

L^2: $m/z = 134$ peak was observed for the C_8H_8NO, OH-C_6H_4–CH═N–CH_2^+. The base peak is observed at $m/z = 100$ for the $C_5H_{11}N_2$, CH_3 attached to morpholine ring. The $m/z = 70$ for the C_4H_6O for the morpholine ring fragmentation.

L^3: $m/z = 111$ peak was observed for the C_6H_7S. The base peak is observed at $m/z = 99$ for the $C_5H_{11}N_2$, CH_3 attached to piperazine ring. The $m/z = 70$ for the $C_3H_6N_2$ for the piperazine ring fragmentation.

L^4: The base peak is observed at $m/z = 99$ for the $C_5H_{11}N_2$, CH_3 attached to piperazine ring. The $m/z = 70$ for the $C_3H_6N_2$ for the piperazine ring fragmentation.

3.3. FTIR spectra

There are some guide peaks such as –CH═N–, –OH, NH, thiophene S and morpholine oxygen whose position or intensities are expected to change upon complexation. The IR spectra of azomethine L^2 and its complexes are shown in Fig. 1. The νC═N stretching vibration of the azomethines are found to be between 1627 and 1633 cm^{-1}. These bands are shifted to lower wavenumbers upon complexation for nickel(II) and iron(II) but higher wavenumbers for Cu(II), indicating coordination of the azomethine nitrogen to metal ions. It is reasonable to infer that after complex formation, C═N possibly reflects a slight difference in the respective C═N bond lengths in copper(II) complexes. FTIR spectra of the ligands show a broad band between 3256 and 3435 cm^{-1}, which can be attributed to phenolic OH groups. This band shifts in all complexes, which could be an indication of involvement in metal complexation. The νC–O stretching bands are observed at about 560 cm^{-1} in L^1 and L^2 and these bands shift to lower or higher wave numbers according to the complexes which is confirmation of M–O involvement [24]. The shift of νC–O to a lower wave number suggests the weakening of C–O and the formation of strong M–O bonds. The N–H stretching wave numbers at about 3135–3200 cm^{-1}in free ligands show considerable shift in all complexes, indicating participation of N–H in all complexes [26]. The IR spectra of all the complexes exhibit a broad band around 3300–3460 cm^{-1}, assigned to ν(OH) of crystalline or coordinated water molecules associated with the complex. This was also confirmed by the thermal and elemental analysis studies. The sharp band at 832, the ν(C–S–C) of thiophene moiety in the L^3 ligand, is shifted to 866–877 cm^{-1} for metal complexes. Therefore, from the IR spectra, it is concluded that azomethines bind to the metal ions; iron(II), copper(II) and nickel(II) with azomethine nitrogen, phenolate O, NH, morpholine oxygen and thiophene sulfur for L^3.

3.4. Thermal analysis of the complexes

Thermal analysis was performed to confirm the elemental analyses and structure of the complexes. The TG curves of the complexes show several steps of decomposition between 25 and 1200 °C (Figs. 2–4). The TG–DTA results of the thermal decompositions of azomethine complexes are given in Table 1. These steps involved mass loss of hydration, counter ions and ligands. There is mass loss up to 200 °C, indicating that either metal bonds or crystal water molecules exist in these complexes [27]. The first mass loss corresponds to the removal of the hydrated water from the complex between 25 and 200 °C. On further heating of the dehydrated complex above 200 °C, the organic part of the complex and counter ions may decompose in one or two steps. These steps leave metal oxides as residue. The DTA results show that all the stages of decomposition were endothermic.

Fig. 7. Color of the Fe L^2 in DMF Acetyl acetone and water.

3.5. Electronic spectra and magnetic susceptibility

The electronic spectra of ligands were measured in methanol and are given in Fig. 5. The aqueous UV–Vis spectra of the azomethine complexes show two absorption bands. One is the charge transfer transition which is observed between 260 and 385 nm and the other one is the d–d transition in between 438 and 641 nm [28]. The measured magnetic moments are in the range 1.55–1.96 BM for the copper complexes indicating the presence of one unpaired electron. A moderately intense band at 357 nm is due to the ligand–metal charge transition [29] and a broad low intensity band at ~500 nm.

The magnetic moment ~1.9 BM falls within the range normally observed for octahedral copper(II) complexes [30]. The nickel(II) complexes are diamagnetic; this is supported by their square planar geometry. Iron(II) complexes are also diamagnetic with octahedral geometry.

3.6. Molar conductivity

The molar conductance of 1×10^{-3} M solution of the complexes was calculated at 20 °C. It is concluded from the results that nickel(II) complexes have molar conductance values between 230 and 248 $\text{S mol}^{-1}\text{ cm}^2$, indicating the ionic character of these complexes; while iron(II) and copper(II) complexes of these ligands have low molar conductivity values between 12 and 23 $\text{S mol}^{-1}\text{ cm}^2$. The nickel(II) complexes are considered to be 2:1 electrolytes with all ligands and chlorides exist as counter ions in the complexes. These data show that iron(II) and copper(II) complexes are non-electrolyte in nature.

3.7. Solvatochromism

The high solubility of FeL^2 complex in various solvents and the change in the color of its solutions from one solvent to another yields solvatochromism. As part of the study on the spectroscopic and thermal characteristics of the azomethines and complexes, the electronic absorption spectra of this complex was measured in a range of organic solvents with different polarities. The UV band of this complex is assigned to the metal-to-ligand charge transfer (MLCT) transition. The promotion of the electron in the low energy orbital of the metal(t_{2g}) to the π^* orbital of the ligand is the MLCT transition. The energy of this band may be affected by solvation of the hydrophobic surface of the azomethine ligand. The position of this band shifted in different solvents, shown in Fig. 6. In pure solvents, the shifts of the $\lambda_{\max}$ values are found to depend on more than one of the known solvent parameters. Acceptor number (AN), donor number (DN), and π^* are found to be the most important solvent parameters, exerting a considerable effect on the solvatochromic shifts of the complex. The color of the FeL^2 complex in different solvents is illustrated in Fig. 7. It is likely that the solvatochromic property of iron(II)–L^2 makes it an important candidate for use in the field of non-linear optics.

4. Conclusions

The structural, electronic, spectroscopic and thermal properties of the ligands and complexes were investigated. The experimental data suggest that tetradentate ligands coordinate to metals via phenolate oxygen, azomethine nitrogen, piperazine nitrogen and morpholine nitrogen and oxygen atoms. The spectroscopic, thermal, conductivity and elemental analysis results indicate that the coordination geometry around the copper and iron center are octahedral consisting of tetradentate basal plane and two chlorides at the axial site while nickel(II) complexes are square planar. All the complexes of different metals decompose in a multi-step process. Some complexes possessing octahedral geometry have a similar mode of degradation to the evolution pattern of inorganic and organic fragments when heated up to 740 °C. Above this temperature corresponding metal oxides are left as residue. Iron and nickel complexes show greater thermal stability, probably owing to less distortion of the octahedral structure and the size of nickel(II) ions. On account of the simplicity of the structure of the aromatic tetradentate complexes, they can be considered a model for studying the relationships between thermal stability, coordination number and chelate ring size for the same metal. The decomposition reaction of aromatic azomethine metal complexes begins with the scission of the M–N bond. A correlation was also found between the thermal stability and the basicity of the ligand. The nature of interaction of the crystallization water plays a significant role in the thermal stability of the metal complexes. The solvatochromic behavior of the iron(II)–L^2 containing N_2O_2 donor set was studied. The charge transfer transition band related to the solvent polarity of the iron(II)–L^2 complex is as follows: DMF (398 nm), AAA (368 nm) and H_2O (328 nm). Solvatochromism is strongly dependent on CT transitions and the nature of π conjugated system, p–π and π–π interaction in the ligand is also responsible. The π conjugated system is a phenyl ring combined with morpholine through the azomethine group in L^2 ligand.

Acknowledgment

We are grateful to COMU, BAP-2010/55 for financial support of this study.

Appendix A. Supplementary material

Supplementary data associated with this article can be found, in the online version, at http://dx.doi.org/10.1016/j.ica.2012.05.006.

References

[1] A Lowson, German patent, DE 2519193 A1, 1975.
[2] A.K. Mishra, N. Manav, N.K. Kaushik, Spectrochim. Acta, Part A 61 (2005) 3097.
[3] K. Nejati, Z. Rezvani, E. Alizadeh, R. Sammimi, J. Coord. Chem. 64 (2011) 859.
[4] O. Kotova, S. Semenov, S. Eliseeva, S. Troyanov, K. Iyssenko, N. Kuzmia, Eur. J. Inorg. Chem. 23 (2009) 3467.
[5] A.A. Nejo, G.A. Kolawole, M.C. Dumbele, A.R. Opoku, J. Coord. Chem. 63 (2010) 4367.
[6] K.M. Vyas, V.K. Shah, R.N. Jadeja, J. Coord. Chem. 64 (2011) 1069.
[7] A.S. Gaballa, M. S Asker, A.S. Bakarat, S.B. Teleb, Spectrochim. Acta, Part A 67 (2007) 114.
[8] K.P. Balasubramanian, K. Parameswari, V. Chinnusamy, R. Prabhakaran, K. Natarajan, Spectrochim. Acta, Part A 65 (2006) 678.
[9] E. Keskinoglu, A.B. Gunduzalp, S. Cete, F. Hamurcu, B. Erk, Spectrochim. Acta, Part A 70 (2008) 634.
[10] V.T. Kasumov, S. Ozalp, E. Tas, Spectrochim. Acta, Part A 62 (2005) 716.
[11] L. Shi, H.M. Ge, S.H. Tan, H.Q. Li, Y.C. Song, H.L. Song, H.L. Zhu, R.X. Tan, Eur. J. Med. Chem. 42 (2007) 558.
[12] A. Pui, J. Pieere, Polyhedron 26 (2007) 3143.
[13] M.M. Omar, G.G. Mohamed, A.A. Ibrahim, Spectrochim. Acta, Part A 73 (2009) 358.
[14] S. Mukhopadhyay, D. Mandal, D. Ghos, I. Goldsberg, M. Chaudhury, Inorg. Chem. 42 (2003) 8439.
[15] Y.G. Li, D.H. Shi, H.L. Zhu, H. Yan, S.W. Ng, Inorg. Chim. Acta 360 (2007) 2881.
[16] P.S. Mukherjee, S. Dalai, G. Mostofa, T.H. Lu, E. Rentschler, N.R. Chaudhuri, New. J. Chem. 25 (2001) 1203.
[17] H.L. Boraley, J. Therm. Anal. Calorim. 73 (2009) 358.
[18] A.S.M. Shirif, H.M. Fattah, J. Therm. Anal. Calorim. 71 (2003) 643.
[19] J. Lv, T. Liu, S. Cai, X. Wang, L. Lu, Y. Wang, J. Inorg. Biochem. 100 (2006) 1888.
[20] Y. Fukuda, Inorganic Chromotropism, Kodansha, Springer, 2007.
[21] W. Linert, Y. Fukuda, A. Camard, Coord. Chem. Rev. 218 (2001) 113.
[22] G. Knör, M. Leirer, T.K. Keyes, J.G. Vos, A. Vogler, Eur. J. Inorg. Chem. (2000) 749.
[23] J. Burgess, C.D. Hubbard, Struct. Chem. 21 (2010) 439.
[24] A. Al-Alousy, J. Burgess, A. Samotus, J. Szklarzewicz, Spectrochim. Acta, Part A 47 (1991) 985.
[25] M.M. Omar, G.G. Mohamed, Spectrochim. Acta, Part A 61 (2005) 929.
[26] C. Chandra, U. Kumar, Spectrochim. Acta, Part A 60 (2004) 2825.
[27] M. El-Beherey, H. El-Twigry, Spectrochim. Acta, Part A 66 (2007) 28.

[28] J. Manonmani, R. Thirumurugan, M. Kandaswamy, M. Kuppayee, S.S.S. Raj, M.N. Ponnuswamy, G. Shanmugam, H.K. Fun, Polyhedron 19 (2000) 2011.
[29] J. Sanmartin, M.R. Bermejo, A.M.G. Deibe, M. Maneiro, C. Lage, A.J.C. Filho, Polyhedron 19 (2000) 185.
[30] F.A. Cotton, G. Wilkinson, C.A. Murillo, M. Bochmann, Advanced Inorganic Chemistry, sixth ed., Wiley, New York, 1999.